Data-Driven Modeling and Control Considering Time Delays for WPT System

Qijun Deng, Zhifan Li, Jiangtao Liu, Shuaiqi Li, Peng Luo, and Kaicong Cui

***Abstract*—A controller for output voltage and power regulation is important for the wireless charging system. For the controller design, it is crucial to establish the accurate system model with considering the time delay, as high time delay exists due to wireless communication, data sampling, and processor calculations for a practical wireless power transfer system. Presently, the common modeling methods, such as the coupled-mode method are based on circuit theories and the component parameters. However, the exact parameters are hard to get due to the diversity of the equipment and application scenarios. Especially, the circuit theories modeling cannot deal with the time delay from hardware limitation and wireless communication. Alternatively, a data-driven modeling method based on the simplified refined instrumental variable method is proposed in this article to get the control-oriented model with time delay. Moreover, based on the estimated model, a controller based on the internal model control is designed to regulate the output voltage. It is shown that the models obtained based on different sampling times are able to accurately describe the system dynamics and the controllers designed based on them are able to achieve the desired control performance.**

***Index Terms*—Modeling and control, refined instrumental variable (RIV) algorithm, time delay, wireless power transfer (WPT).**

I. Introduction

WIRELESS power transfer (WPT) technology has gained much attention since the strongly coupled magnetic resonance WPT was proposed in 2007 that a new breakthrough was made in mid-range energy transmission [1]–[3]. The last decade has witnessed the surge of this promising technology in all sorts of fields, such as electric vehicles [4], [5], implantable bioelectronics [6], [7], and laptops [8].

The removal of cable enables consumers to obtain improved security, feasibility, and robustness for scenarios when power cable connections are not allowed. Meanwhile, new challenges for analysis, control of the WPT system arise for its effective operation [9]. One of the pressing challenges is the modeling and control of WPT systems with time delays. The presence of time delay can result in poor accuracy in system modeling and controller design. Consequently, this article focuses on the modeling and the control of WPT systems with time delay.

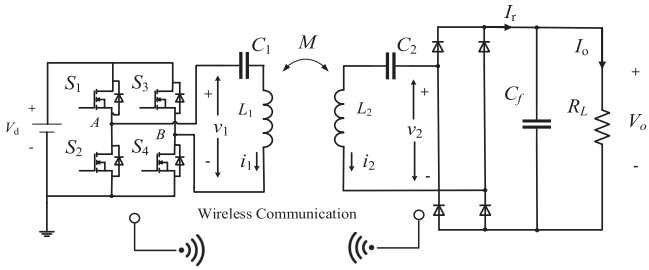

Fig. 1. Scheme of S–S compensated WPT with communication time delay.

This article aims at the analysis of WPT systems with the time delay, which is depicted in Fig. 1. Time delay frequently occurs in industrial applications due to hardware limitation and wireless communication. There are already a few articles investigating the time-delay feature of WPT. In [10], the time delay of the WPT system was analyzed. However, this article only considered this issue in the laboratory environment where the wireless communication was not used and the time delay was very small and was ignored at last. Irrespective of the data-driven modeling method on the system-level, the time delay was also considered on the circuit-level in [11]. To improve the accuracy of the zero-voltage switching angel control, a uniform time-delay compensation method (UTDCM) is proposed. However, to implement UTDCM, various parameters such as driven delay, dead time delay and so on should be prior known, which requires accurate experimental measurement. The purpose of this article is to acquire the accurate control model parameters with time delay and exert effective control for the WPT system.

The accurate model that can describe the input-output behavior with the time delays of the system would be necessary for control design. The circuit-theory modeling methods, such as the coupled mode theory [12], the equivalent small parameter method (ESPM) [13], state-space method [14], and so on, have been proposed to derive the mathematical models. However, in practical industrial applications, due to the diverse components from different manufactures or the variation of the coil placement in different spots, the actual parameters may drift

Manuscript received June 23, 2021; revised December 15, 2021; accepted February 3, 2022. Date of publication February 16, 2022; date of current version April 28, 2022. This work was supported by the National Natural Science Foundation of China under Grants 51907054 and 51977151. Recommended for publication by Associate Editor U. K. Madawala. *(Corresponding authors: Zhifan Li; Jiangtao Liu.)*

Qijun Deng, Zhifan Li, Shuaiqi Li, Peng Luo, and Kaicong Cui are with the School of Electrical Engineering and Automation, Wuhan University, Wuhan 430072, China (e-mail: dqj@whu.edu.cn; lizhifan@whu.edu.cn; lishuaiqi@whu.edu.cn; luo.peng@whu.edu.cn; kaicong.cui@whu.edu.cn).

Jiangtao Liu is with the School of Physical, Mechanical and Electrical Engineering, Hubei University of Education, Wuhan 430205, China (e-mail: liu_jiangtao@whu.edu.cn).

Color versions of one or more figures in this article are available at https://doi.org/10.1109/TPEL.2022.3151941.

Digital Object Identifier 10.1109/TPEL.2022.3151941

from the rated value. Additional, the order of the circuit-theory-based model is commonly high which gives rise to difficulty for control design. Besides, the traditional modeling strategy does not pay much attention to the time delays. For a practical WPT system, however, the wireless communication for output feedback at the secondary side is commonly employed, where the communication time delay has a large effect for the modeling and controller design. In this case, the conventional methods are not good choices for WPT modeling.

To solve this problem, an alternative data-driven modeling method is adopted to infer models of WPT systems. The data-driven modeling based on experimental data is able to yield simple models suited for control design. In this article, the transfer function (TF) model with time delays is characterized to describe the dynamic behavior of the system.

There are various techniques have been devised to straightforwardly estimate the parameters in a continuous-time (CT) transfer function model, such as the linear least-squares (LS) method, the instrumental variable (IV) method [15], and the prediction error method [16]. The main advantage of IV methods lies in that they provide a simple LS-like solution, and the resulting parameter estimates can still be consistent even in the presence of measurement noise [17]. In particular, the time-derivative terms needed in the estimation process are not available for direct measurement. Some prefiltering such as the standard IV methods were proposed to handle it. Although the sub-optimal methods are useful to some extent because their prefilters are simple to implement, it will not be considered in this article since the optimal simplified refined instrumental variable (SRIV) algorithm is more robust in the general use. The development of the RIV algorithm was realized by Young and Jakeman in 1980 [18]. The optimal RIV algorithm was developed in a *Simplified* (SRIVC) form [15], which is optimal in the case of white additive noise and will be used to estimate the rational model parameters in this article. Time delay, which is a nonlinear term, will complicate the estimation process. Therefore, the time-delay identification is separated from the model parameter estimation. Based on the SRIVC algorithm, the time delay is defined and selected by comparing performance index of several practical evaluation methods.

Moreover, a controller based on internal model control (IMC) is designed to regulate the output voltage. IMC is a kind of control algorithm based on mathematical model. It has the features of simple design, easy adjustment, robustness, and good control effect, especially it has good compensation for pure time delay [19]. According to the IMC theory, the model will be divided into two parts, one containing the time delay and the unstable part of the model, and the other the stable part of the model.

This article extends the research in [10] and emphasizes on the time-delay feature of the WPT systems. The contributions of the article are threefold and as follows.

1) The combination of the system identification and IMC is proposed. It provides a user-friendly and effective way to regulate the output of the WPT system, which means the user does not need to know the exact component parameters and experience troublesome parameter adjustment.

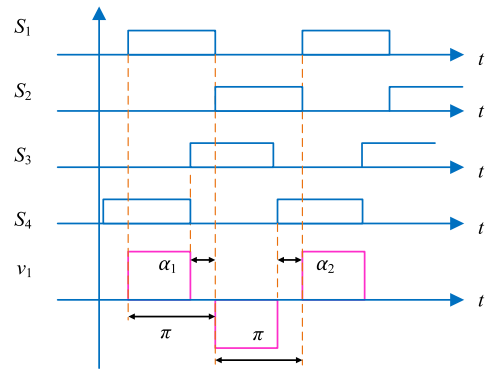

Fig. 2. Waveforms of the control signals for switches S_1–S_4, respectively. v_1 is the input voltage of the resonant tank.

2) The effect of sampling interval on time-delay estimation has been investigated. Based on different sampling intervals, the evaluated time delay is various. However, with the estimated parameters, the resulting models in different sampling cases can all well depict the dynamic behavior of the WPT system based on the proposed data-driven modeling method.
3) The controller performance under various resulting models is also studied. All controllers based on various models all can achieve the desired control performance, even these models are resulting from different sampling intervals together with corresponding evaluated time delays.

The rest of this article is organized as follows. Section II introduces the single-input single-output (SISO) series–series (S–S) WPT system and the estimation algorithm. Then, a new IMC theory based on the SRIV estimation and simulation are presented in Section III. Subsequently, experimental examples are shown in Section IV to verify the effectiveness of the proposed method. Finally, Section V concludes this article.

II. Theoretical Analysis of Data-Driven WPT Modeling

A. WPT System

A typical topology of a SISO, S–S compensated WPT system is considered in this article, as shown in Fig. 1. In this figure, V_d is a dc voltage source, L_1 and L_2 are two coil inductors, which are compensated by C_1 and C_2, respectively. C_f is an output filter capacitor, and R_L is the load resistance. The input stage is a full-bridge inverter, see Fig. 2 for the typical signal waveforms generated in the circuit, where v_{S1}–v_{S4} denote the control signals for switches S_1–S_4. To adjust the output voltage V_o, the control variable $\alpha = \alpha_1 + \alpha_2$, which is commonly called as control angle, is chosen as the phase between adjacent switching legs to regulate the duty cycle of S_1–S_4. When $\alpha < 0.5\pi$, $\alpha_1 = \alpha$, α_2 is set to 0 and the duty cycle of S_1 and S_2 is fixed at 50%. When $\alpha > 0.5\pi$, α_1 is set to 0.5π and $\alpha_2 = \alpha - 0.5\pi$. As α changes from 0 to π, the output voltage of the inverter gradually decreases from the maximum to zero. This control strategy is known as the optimal ZVS modulation strategy, which

has a larger adjustable control angle range than the traditional phase-shift control method for maintaining ZVS. The control method can be written as

$$0 \le \alpha \le 0.5\pi \begin{cases} \alpha_1 = \alpha \\ \alpha_2 = 0 \end{cases} \quad 0.5\pi < \alpha \le \pi \begin{cases} \alpha_1 = 0.5\pi \\ \alpha_2 = \alpha - 0.5\pi. \end{cases}$$

Note that the resonant tank is highly frequency selective, then only the first harmonic of v_1 can pass through [20].

In [10], it is proposed that the parsimonious structure of the WPT system can be derived based on the dominant mode analysis. Therefore, the S–S model can be described by a low-order model, which is enough to capture the low-frequency behavior of the whole system

$$V_o = \mathrm{KG}(s) f(\alpha) \tag{1}$$

where K is the scaling factor, $G(s)$ is a low-order transfer function model with s the Laplace transfer operator, and $f(\cdot)$ is a static-input nonlinearity function.

For control system design, the linear models are preferred, so a linearized, small-signal model at the given set point is considered in this article. Therefore, the signal should be decomposed as a static value plus a small signal as

$$V_o = \overline{V}_o + \tilde{V}_o \;\; \alpha = \overline{\alpha} + \tilde{\alpha} \tag{2}$$

where $\overline{V}_o$ and $\overline{\alpha}$ denote the static value, $\tilde{V}_o$ and $\tilde{\alpha}$ denote the small signal parts. Using the first-order Taylor expansion, we can obtain the following expression:

$$\tilde{V}_o = \mathrm{KG}(s) \frac{\partial f(\alpha)}{\partial \alpha}\bigg|_{\alpha=\overline{\alpha}} \tilde{\alpha}. \tag{3}$$

In practical engineering applications, time delays commonly exist in WPT systems due to hardware limitation, for example, when the control signals pass the optocouplers, or when the measured output is sent to the host controller via wireless communication. The ignorance of time delay can degrade the modeling accuracy or depress performance of controller. If the total delay is close to or even greater than the sampling period, the impact of the time delay on the model needs to be taken into account for the controller design. According to [21], the total delay of the communication is about 0.4 ms. Considering other effects, the total time delay can reach 1 ms. When the sampling time of the controller is about 1 ms, the time delay of the model cannot be ignored. Otherwise, the accuracy of the modeling will be much lower.

For the brevity of introduction, the output voltage $\tilde{V}_o$ and control angle $\tilde{\alpha}$ are replaced by x and u. Based on these, as a more general version of (3), the Box-Jenkins (BJ) model with time delay τ is used to describe the input–output behavior of the system

$$\begin{cases} x(t) & = G(s,\theta)u(t-\tau) = \frac{B(s,\theta)}{A(s,\theta)}u(t-\tau) \\ y(t_k) & = x(t_k) + e(t_k) \end{cases} \tag{4}$$

with

$$\boldsymbol{\theta} = [a_1, \ldots, a_n, b_0, \ldots, b_m]^T$$

$$A(s,\boldsymbol{\theta}) = s^n + a_1\, s^{n-1} + \cdots + a_n$$

$$B(s,\boldsymbol{\theta}) = b_0\, s^m + b_1\, s^{m-1} + \cdots + b_m$$

where s and τ denote the differential operator and the time delay, respectively. $\{e(t_k)\}$ is the white noise sequence. The experimental signal is sampled regularly at the time instant $t_k = kT_s, k \in \mathbb{N}^+$, where T_s is the sample time. Then, the objective is to estimate the parameter vector $\boldsymbol{\theta}$ and the time delay τ from the sampled data$\{y(t_k), u(t_k)\}_{k=1}^N$.

B. Estimation Algorithm

Before the identification algorithm is applied to estimate the parameter vector θ, the structure of the transfer function model needs to be decided. In this article, the structure not only involves the orders of the polynominals $A(s,\boldsymbol{\theta})$ and $B(s,\boldsymbol{\theta})$, which is the value of n and m, but also includes τ, the time delay of WPT system. The model structure can be defined by the triad $[n \;\; m \;\; \tau]$. Therefore, the data-driven modeling will be divided into following two parts

1) Time-Delay Estimation: In this article, first-order and second-order models will also be used to investigate and control the system. Besides, the main challenge is to determine the time delay. There are several practical evaluation methods will be used below. Finally, the time delay is determined by their synthesized indicators (R_T^2 and YIC).

The first index is known as coefficient of determination R_T^2, which stems from regression analysis.

$$R_T^2 = 1 - \frac{\frac{1}{N}\sum_{k=1}^N (\hat{e}(k) - \bar{\hat{e}}(k))^2}{\frac{1}{N}\sum_{k=1}^N (\hat{y}(k) - \bar{\hat{y}}(k))^2} \tag{5}$$

where $\bar{e}(k)$ is the error between the simulated TF model output $\hat{x}(k)$ and the measured output $y(k)$.

R_T^2 is able to capture the extent to which the deterministic part of the TF model affects the variance σ_y^2. It is important because it indicates the effect of the input $u(k)$ on the output. But one of the shortcomings of the R_T^2 is that this index can result in the overparameterization since overparameterized models usually explain the data well. Therefore, to get a parsimonious model, we cannot use R_T^2 alone.

The young information criterion (YIC) is a heuristically defined identification criterion. It can only be used with IV-type algorithms since it exploits the instrumental product matrix (IPM) used in IV algorithms

$$IPM = \sum_{i=1}^{k} \hat{\phi}(i)\phi^T(i). \tag{6}$$

For a sample size N, the YIC criterion can be expressed as

$$\mathrm{YIC} = \log_e \left\{ \frac{\sigma^2}{\sigma_y^2} \right\} + \log_e \mathrm{EVN} \tag{7}$$

$$\mathrm{EVN} = \frac{1}{n_p} \sum_{n_p}^{i=1} \frac{\hat{\sigma}^2 \rho_{ii}}{\hat{\rho}_i^2} \tag{8}$$

where $n_p (n_p = n + m + 1)$ is the number of parameters in the $\boldsymbol{\theta}$ vector; ρ_{ii} are the diagonal elements of the inverse IPM, which

is the $P(N)$ matrix generated by SRIVC algorithm; and $\hat{\rho}_i$ are SRIVC parameter estimates. The logarithmic term measures how well the model explains the data: the smaller the model residuals the more negative the term becomes. The second term provides a logarithmic measure of the conditioning of the IPM. Once the model is overparameterized, the IPM will tend to singularity and the elements of its inverse $P(N)$ will increase in value. When this happens, the second term tends to dominate the criterion function.

After introducing the above-mentioned statistical measures, this article develops a useful approach to estimate the time delay when using the SRIVC algorithm.

a) Specify a range of different models for $\min(\tau) \leq \tau \leq \max(\tau)$, $n = 1$ and $m = 1, 2$, where the minimum and the ranges of n, τ, and m are selected by the user.
b) Then, the rational parameters of the models are estimated by SRIVC algorithm.
c) Finally, sort these models by the value of R_T^2, choose a model with high R_T^2 and low YIC value, then, the most suitable evaluated time delay is decided. Do not select a model with high R_T^2 and large YIC value, which may bring overparameterization.

2) Rational Parameter Estimation: When degrees n, m, and τ are known, the identification problem is to estimate the parameter vector $\boldsymbol{\theta}$ by minimizing the output-error loss function

$$\hat{\boldsymbol{\theta}} = \arg\min_{\boldsymbol{\theta}} J(\boldsymbol{\theta}) \tag{9}$$

$$J(\boldsymbol{\theta}) = \sum_{k=1}^{N} \varepsilon(k)^2 = \sum_{k=1}^{N} [y(t_k) - \frac{B(p,\boldsymbol{\theta})}{A(p,\boldsymbol{\theta})} u(t-\tau)]^2. \tag{10}$$

Various methods have been proposed to solve the above-mentioned estimation problem, such as the LS methods, the prediction error methods, the instrumental variable (IV) methods and so on. Here, the IV method is adopted to estimate the parameter vector $\boldsymbol{\theta}$. Particularly, the SRIV algorithm for CT models (SRIVC), where the noise is represented by the white noise, is used here. The error function $\varepsilon(k)$ can be defined as follows:

$$\begin{aligned} \varepsilon(t_k) &= y(t_k) - \frac{B(p,\boldsymbol{\theta})}{A(p,\boldsymbol{\theta})} u(t_k - \tau) \\ &= A(p,\boldsymbol{\theta}) y_f(t_k) - B(p,\boldsymbol{\theta}) u_f(t_k - \tau) \end{aligned} \tag{11}$$

where the subscript f denotes the associated variables have been prefiltered by $f(p,\boldsymbol{\theta}) = \frac{1}{A(p,\boldsymbol{\theta})}$. Subsequently, the model can written to the pseudolinear form [22]

$$y_f(t_k) = \boldsymbol{\phi}^T(t_k)\boldsymbol{\theta} + e(t_k) \tag{12}$$

where

$$\begin{aligned} \boldsymbol{\phi}^T(t_k) = [&-y_f^{(n-1)}(t_k) \ldots - y_f^{(0)}(t_k) \\ &u_f^{(m)}(t_k - \tau) \ldots u_f^{(0)}(t_k - \tau)]. \end{aligned}$$

Although the model seems to be linear in $\boldsymbol{\theta}$ from (12), the LS estimate will be biased because $\boldsymbol{\phi}^T(t_k)$ is correlated with the noise $e(t_k)$. In order to get the asymptotically unbiased estimate of $\boldsymbol{\theta}$, the SRIV algorithm is adopted

Algorithm 1: SRIVC Algorithm.

Input :
- Sampled data:$\{y(t_k), u(t_k)\}_{k=1}^N$;
- Polynomial degrees and time-delay:$\{n, m, \tau\}$;
- Maximum iteration number: $N_{\max}$;
- Initial parameter vector: $\boldsymbol{\theta}_0$;

Output: Parameter vector, $\boldsymbol{\theta}$;

for $j = 1$ **to** $N_{\max}$ **do**
- Generate the IV variable $\hat{x}(t_k)$ from the auxiliary model: $\hat{x}(t_k) = \frac{\hat{B}(p,\boldsymbol{\theta}^{(j-1)})}{\hat{A}(p,\boldsymbol{\theta}^{(j-1)})} u(t-\tau)$.
- $\boldsymbol{\theta}^{(j-1)}$ denotes the estimated parameter vector obtained at the previous iteration;
- Prefilter the input $u(t)$, output $y(t)$ and the instrument variable $\hat{x}(t)$ by the continuous filter: $f_c(p,\boldsymbol{\theta}^{(j-1)}) = \frac{1}{\hat{A}(p,\boldsymbol{\theta}^{(j-1)})}$ to generate the filtered derivatives shown in (12);
- Generate the estimate $\boldsymbol{\theta}^{(j)}$ using the IV estimator in (13);

end

$$\hat{\boldsymbol{\theta}}(t_k) = \hat{\boldsymbol{\theta}}(t_k - 1) + \boldsymbol{g}(t_k)[y_f(t_k) - \boldsymbol{\phi}^T(t_k)\hat{\boldsymbol{\theta}}(t_k - 1)] \tag{13a}$$

$$\boldsymbol{g}(t_k) = \frac{\hat{\boldsymbol{P}}(t_k - 1)\hat{\boldsymbol{\phi}}(t_k)}{\sigma^2 + \boldsymbol{\phi}^T(t_k)\hat{\boldsymbol{P}}(t_k - 1)\hat{\boldsymbol{\phi}}(t_k)} \tag{13b}$$

$$\hat{\boldsymbol{P}}(t_k) = \hat{\boldsymbol{P}}(t_k - 1) - \boldsymbol{g}(t_k)\boldsymbol{\phi}^T(t_k)\hat{\boldsymbol{P}}(t_k - 1) \tag{13c}$$

where $\hat{\boldsymbol{P}}(t_k)$ is the estimated error covariance matrix and $\hat{\boldsymbol{\phi}}(t_k)$ is the instrumental vector specified by the user, which is uncorrelated with $e(t_k)$ but maximally correlated with $\boldsymbol{\phi}(t_k)$. It is defined as follows:

$$\begin{aligned} \hat{\boldsymbol{\phi}}(t_k) = [&-\hat{x}_f^{(n-1)}(t_k) \ldots - \hat{x}_f^{(0)}(t_k) \\ &u_f^{(m)}(t_k - \tau) \ldots u_f^{(0)}(t_k - \tau)] \end{aligned}$$

where $\hat{x}_f(t_k)$ is the prefiltered output of the auxiliary model

$$\hat{x}(t_k) = \frac{\hat{B}(p,\boldsymbol{\theta})}{\hat{A}(p,\boldsymbol{\theta})} u(t_k - \tau) \tag{14}$$

where $\hat{A}(p,\boldsymbol{\theta})$ and $\hat{B}(p,\boldsymbol{\theta})$ are the iteratively updated estimates of the system TF model polynomials. The SRIVC algorithm is summarized in Algorithm 1.

III. Controller Design and Simulation Example

As a mathematical model-based control algorithm, IMC has a relatively simple design process with fewer parameters, greater robustness, and the ability to compensate for time delay. Notably, it can be effectively combined with the BJ model with pure time delays obtained by system identification. By converting the internal-mode controller into a PI controller, an IMC-PI controller is then obtained.

A. IMC Scheme for SISO Output Voltage

The purpose of IMC is to introduce a reference model in the control system and connect it in parallel with the controlled object. The controller is designed according to the inverse of the reference model, and to further improve the robustness of the system, a filter is added to the control system.

B. Controller Design

The design steps of IMC are as follows: the reference object $G_m(s)$ should be decomposed as $G_{m+}(s)$ and $G_{m-}(s)$

$$G_m(s) = G_{m+}(s)G_{m-}(s) \tag{15}$$

where $G_{m-}(s)$ is the minimum phase part of the reference model, $G_{m+}(s)$ is the nonminimum phase part, which contains the time-delay part and the zeros in the right half-plane. As for a first-order model with time delay, they can be denoted as

$$G_{m-}(s) = \frac{b}{s+a}$$
$$G_{m+}(s) = e^{-\tau s}$$

where τ is the time delay, a and b are the estimated parameters of the first-order model. Then, the IMC controller $Q(s)$ can be expressed as

$$Q(s) = G_{m-}(s)F(s) \tag{16}$$

$$F(s) = \frac{1}{(1+\lambda s)^r} \tag{17}$$

where $F(s)$ is a low-pass filter. r is usually set to 1. λ is the parameter of the filter, which is the only adjustable parameter of IMC. The smaller the λ, the faster the closed-loop response of the system, and vice versa, the slower the closed-loop response. Its characteristic will be further discussed in the experiment. After an equivalent transformation, the IMC controller can be converted to a unit feedback PI controller $G_c(s)$

$$G_c(s) = \frac{Q(s)}{1 - Q(s)G_m(s)} = \frac{G_{m-}^{-1}(s)}{\lambda s + 1 - e^{-\tau s}}. \tag{18}$$

In order to make the controller structured as a PI controller, the time-delay term is approximated by a first-order Taylor expansion as follows:

$$\mathrm{e}^{-\tau s} \approx 1 - \tau s. \tag{19}$$

According to (18) and (19), the IMC controller can be shown as

$$G_c(s) = \frac{G_{m-}^{-1}(s)}{\lambda s + 1 - 1 + \tau s} = \frac{1}{b(\lambda+\tau)} + \frac{a}{b(\lambda+\tau)}\frac{1}{s}. \tag{20}$$

Then, $G_c(s)$ can be written in a PI form

$$G_c(s) = K_p\left(1 + \frac{1}{T_I s}\right) \tag{21}$$

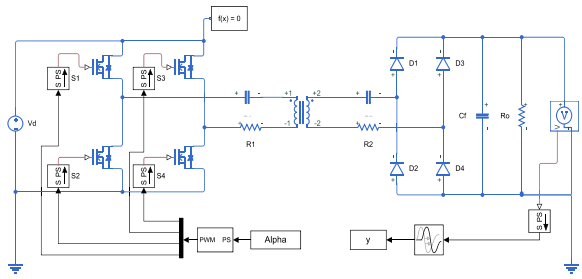

Fig. 3. Simulink diagram for simulation.

TABLE I
MAIN PARAMETERS

Parameter	Explanation	Value
L_1	Inductance of the sending resonator	110 μH
L_2	Inductance of the receiving resonator	110 μH
M	Mutual inductance between L_1 and L_2	33 μH
C_1	Capacitance of the sending resonator	26 nF
C_2	Capacitance of the receiving resonator	25.4 nF
C_f	Capacitance of the output filter	600 μF
R_o	Load Resistance	33 Ω
V_d	Voltage of the dc voltage	500 V
f_s	Switching frequency of the inverter	82kHz
τ	Time-delay of the system	1.2 ms
R_1	Equivalent resistance of the L_1, C_1 branch	39 mΩ
R_2	Equivalent resistance of the L_2, C_2 branch	39 mΩ

where $K_p = \frac{1}{b(\lambda+\tau)}$ and $T_I = \frac{1}{a}$.

C. Simulation Example

In this section, the effectiveness of the data-driven modeling and IMC methods are verified by means of numerical simulation in MATLAB (2017b). The circuit diagram to generate data for identification is shown in Fig. 3: see Table I for the main component parameters. Besides, 1.2 ms pure time delay is added before the acquisition of the output voltage to simulate real working conditions by implementing a transport time-delay module. The input u is injected through the 'Alpha' module, and the data in y are collected to form the dataset used for identification.

Before collecting the sampled data, the system should operate at a stationary state. The input can be decomposed as a static value plus a small signal static input as $\alpha = \bar{\alpha} + \tilde{\alpha}$. When $\bar{\alpha} = 0.1\pi$ rd, the static voltage output is $\bar{V}_o = 502$ V. To acquire useful data for identification, the input $\tilde{\alpha}$ is chosen as a M-sequence with amplitude switching between $\pm 0.06\pi$ rd generated from a five-stage shift register at a clock period $5T_s$, where $T_s = 0.1$ ms is the sampling interval. The input–output data are collected at $t_k = kT_s, k = 1, \ldots, 3600$. The measured ouput $Y(t_k)$ is corrupted by white noise $e(t_k)$.

$$y(t_k) = x(t_k) + e(t_k). \tag{22}$$

After obtaining the sampled data $\{y(t_k), u(t_k)\}_{k=1}^{3600}$, first, the structure including time delay needs to be decided. Specify a range of different models for $n = 1$, $1 \le m \le 2$ and $5 \le \tau \le 20T_s$ and select the best one from the 32 models according to the criterion mentioned in Section II, which is based on the CONTSID toolbox for MATLAB.

TABLE II
SIMULATION RESULTS

$[n \quad m \quad \tau]$	R_T^2	YIC	fit
$[1 \quad 1 \quad 12T_s]$	0.985	-13.67	88.37 %
$[1 \quad 2 \quad 12T_s]$	0.995	-14.30	93.93 %
$[1 \quad 1 \quad 0]$	-	-	67.60 %
$[1 \quad 2 \quad 0]$	-	-	73.71 %

TABLE III
FIT RATIOS FOR DIFFERENT SAMPLING TIME

Sampling time	Evaluated delay τ	Fit
0.1ms	1.2ms	88.14 %
0.2ms	1.2ms	87.98 %
0.5ms	1.5ms	86.15 %
1.0ms	1.0ms	85.68 %
1.2ms	1.2ms	90.18 %
2.0ms	0.0ms	83.68 %

Then, the best structures of the system are set to be $[1 \quad 1 \quad 12T_s]$ and $[1 \quad 2 \quad 12T_s]$, which verify the analysis in Section II. The exact index of the two structures are listed in Table II. Estimated by the SRIVC algorithm, the first-order model with time delay is

$$G_1 = \frac{-4.357e5}{s + 696} u(t - 1.2e^{-3}). \tag{23}$$

The estimated second-order model is

$$G_2 = \frac{-1.271e9}{s^2 + 2889s + 2.062e6} u(t - 1.2e^{-3}). \tag{24}$$

The accuracy of the abovementioned estimated model is evaluated by the performance index

$$\text{fit} = \left(1 - \frac{||y(t_k) - y_s(t_k)||_2}{||y(t_k) - y_m(t_k)||_2}\right) \times 100\% \tag{25}$$

where $y(t_k)$ is the sampled output, $y_s(t_k)$ is the simulated output calculated by the estimated model, and $y_m(t_k)$ is the mean value of $y(t_k)$. The fit ratios of the estimated models (23) and (24) are 88.37% and 93.93%, respectively. If time delay is not taken into account, the first-order model and second-order model will be poorly identified with the fit ratios of 67.6% and 73.7%, respectively, so it can be seen that time-delay identification is necessary for WPT systems with wireless communication.

Besides, the length of the sampling time also influences accuracy for the identification of the time delay. Since the identified time delay can only be an integer multiple of the sampling time. For the WPT system shown in Table II, with different sampling times, the obtained time delay and the fit ratios of the models with the same order are shown in Table III. One can see from Table III that as the sampling time increases, the fit ratio of the model gradually decreases (except that the sampling time is exactly equal to the assumed time delay 1.2 ms). When the sampling interval is lower than the practical time delay at the order of magnitude, the time delay can be accurately estimated. On the contrary, when the sampling interval is closed to the practical time-delay, errors of integer multiples of the sampling interval are introduced (error is usually between 0 and a sampling interval).

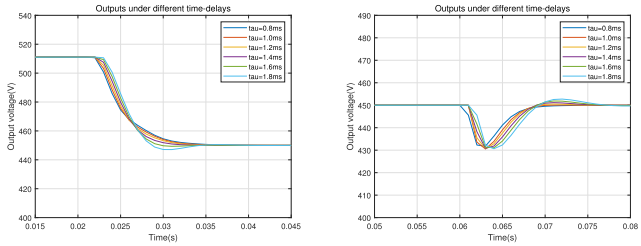

Fig. 4. V_o control simulation for different time delays. (a) Reference voltage changes. (b) Load changes.

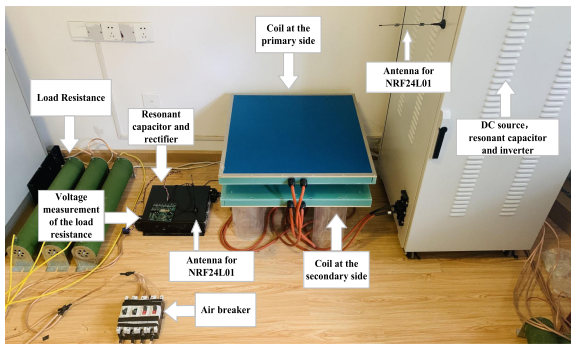

Fig. 5. Prototype of the S–S WPT system.

Besides, the control performance of the system does not change significantly when small changes in time delay occur. On the one hand, the controller is robust, which is verified by means of numerical simulation in MATLAB. Based on (20) and the estimated model ($T_s = 1$ ms), the internal model controller is acquired. (The control period is set to be 1 ms.) The outputs when the reference voltage and load changes under different time delays are shown in Fig. 4. It can be seen that the control performances with the same controller under different time delays are similar. The proposed controller design method still works when the time delay slightly varies. If the controller performance deteriorates due to excessive delay variation, the user can recollect a period of experimental data to update the controller parameters, which will only take a little time.

IV. EXPERIMENTAL VERIFICATION

A. Prototype Design

An S–S compensated WPT prototype is shown in Fig. 5. The prototype consists of a dc source, a full-bridge inverter, resonant coils, resonant capacitor banks, a rectifier, and a resistive load at the receiving side.

1) For the full-bridge inverter, its power stage is mainly composed of four SiC MOSFETs of IMW120R045M1. The inverter is powered by an adjustable dc source of REG75030. Two CPUS, namely, ARM of STM322F407VGT and FPGA of XC6SLX9-3TQG1441 consist the control board for the inverter. The ARM implements the IMC based on the data from the wireless module and outputs control

TABLE IV
COMPONENT PARAMETERS

Parameter	Explanation	Value
L_1	Inductance of the sending resonator	117 μH
L_2	Inductance of the receiving resonator	116 μH
M	Mutual inductance between L_1 and L_2	36.5 μH
C_1	Capacitance of the sending resonator	26 nF
C_2	Capacitance of the receiving resonator	25.4 nF
C_f	Capacitance of the output filter	60 μF
R_o	Load Resistance	33 Ω
V_d	Voltage of the dc voltage	500 V
f_s	Switching frequency of the inverter	82 kHz
T_s	Sampling time	1 ms
R_1	Equivalent resistance of the L_1, C_1 branch	186 mΩ
R_2	Equivalent resistance of the L_2, C_2 branch	198 mΩ

angle to the FPGA, which provides driver signals for MOSFETS. The output voltage is sampled by a measured PCB with an ARM of STM322F407VGT and is transferred to the control board via wireless communication modules of nRF24L01.

2) The rectangular resonant coils with a gap of 10 cm and nine turns wound by Litz wire are the same for the both sides. The Litz wire is composed of 3000 insulated strands. The inner and outer width of each resonant coil are 62 and 70 cm, respectively. PC40 ferrite cores with 10 × 10 cm × 5 mm and aluminum sheets of 80 × 80 cm are employed to shield the leakage magnetic.
3) Tow polypropylene resonant capacitors, 10 and 16 nF from DAWNCAP are connected parallel to compensate the inductance. The full-bridge rectifier at the receiving side adopts four SiC Schottky Diode of IDW40G120C5B.
4) Component parameters listed in Table IV are measured by a Keysight E4980AL LCR.

B. Experimental Procedure

1) Model Estimation

a) First, letting, the stationary input, $\bar{\alpha} = 0.1$, the steady-state output voltage is measured as $\bar{V}_o = 514$ V. At this working point, the input power is $500\text{V} \times 16.84\text{A} = 8.42\text{kW}$. Therefore, the efficiency of the prototype can be calculated as $514^2/33.3/8420 \times 100\% = 94.23\%$.
b) Second, the small signal $\tilde{\alpha}$ is chosen as a PRBS of amplitude switching between ± 0.06 to persistently excite the system, which is generated by a four-stage shift register at a clock period of 10 T_s, where $T_s = 1\text{ms}$ is the sampling interval.
c) Finally, during the process of applying the PRBS sequence, the input–output data are collected at the sampling instant $t_k = kT_s, k = 1, \ldots, 3000$.
The input–output data with 3000 sampling points are uploaded to the private compute for system identification.

Before estimating the rational model parameters, the data is analyzed following the steps in Section II to determine the orders and the time delay of the system. After calculation, the structure of this system is decided to be $[1 \quad 1 \quad 1]$, the $R_T^2 = 0.9857$ YIC

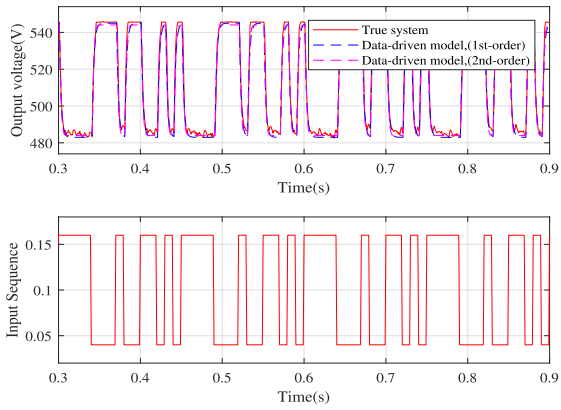

Fig. 6. Portion of sampled input–output experimental data.

TABLE V
FIT RATIOS FOR DIFFERENT SAMPLING TIME IN EXPERIMENT

Sampling time	Evaluated delay τ	Fit
0.8ms	1.6ms	86.75%
1.0ms	1.0ms	88.20%
1.2ms	1.2ms	87.91%
1.5ms	1.5ms	87.78%

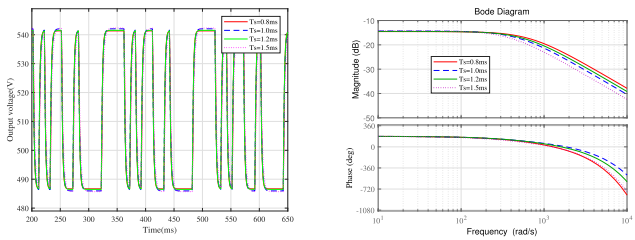

(a) (b)

Fig. 7. Comparison of estimated models based on different sampling intervals. (a) Outputs under the same PRBS. (b) Bode diagram.

$= -13.37$. The estimated first-order model is

$$x(t) = \frac{-105.6}{s + 497} u(t - 0.001) \tag{26}$$

with the fit ratio being 88.2%. The estimated second-order model is

$$x(t) = \frac{-2.238e5}{s^2 + 2055s + 1.087e6} u(t - 0.001) \tag{27}$$

with the fit ration being 90.59%. A portion of the input–output data is shown in Fig. 6. The solid line represents the experimental data, while the dashed lines denote the simulation outputs of the low-order models for the same PRBS. It can be seen that both models can explain the data very well, which indicates that a first-order model is sufficient to provide good explanation of the experimental data.

It should be note that the estimation results do not reach the Cramer–Rao lower bounds. But in the following control experiment, based on the estimated model, the control performance is satisfactory. The estimation accuracy may be higher at a finer sampling interval and considering the noise model. A short

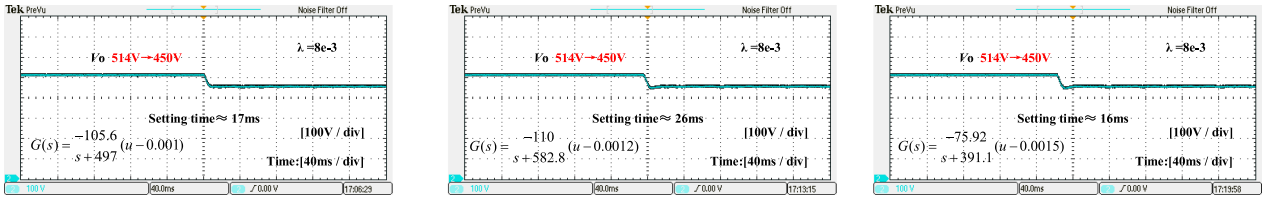

(a) (b) (c)

Fig. 8. V_o control experiment for the reference voltage decreases for different sampling intervals, when $\lambda = 8e-3$. (a) $T_s = 1.0$ ms. (b) $T_s = 1.2$ ms. (c) $T_s = 1.5$ ms.

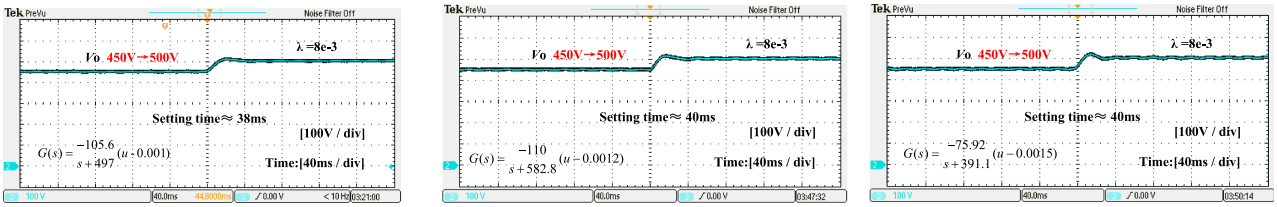

(a) (b) (c)

Fig. 9. V_o control experiment for the reference voltage rises for different sampling intervals, when $\lambda = 8e-3$. (a) $T_s = 1.0$ ms. (b) $T_s = 1.2$ ms. (c) $T_s = 1.5$ ms.

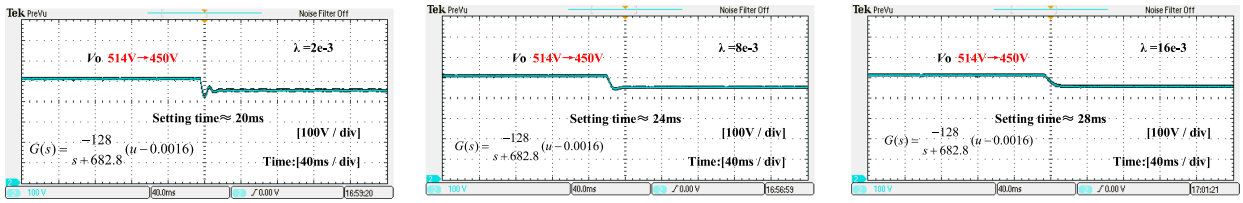

(a) (b) (c)

Fig. 10. V_o control experiment for the reference voltage decreases for different λ, when $T_s = 0.8$ms, $\tau = 1.6$ms. (a) $\lambda = 2e-3$. (b) $\lambda = 8e-3$. (c) $\lambda = 16e-3$.

sampling interval and RIVC algorithm would be preferable if it were available. But considering the hardware limitation and the feasibility of the proposed method, the user can adopt 1 ms sampling interval and SRIVC algorithm, which is sufficient to meet the control requirements.

As discussed before, the length of the sampling interval has an impact on the time-delay identification, so the experimental data is sampled based on different sampling intervals, and the identification results are shown in Table V (the minimum value of sampling interval is 0.8 ms due to the limitation of the communication rate of the wireless module). When T_s increases from 1 to 1.5 ms, the fit ratio gradually reduces, which confirms the deduction of the simulation, but the difference is not significant. Besides, the estimated time delays are various when sampling intervals are different. The practical time delay of the system is approximately between 0.8 and 1.2 ms as the resulting 1.0 ms time delay shows the highest fit. In fact, the dynamic behavior of the model are determined by a combination of the model's time delay as well as the rational parameters. After the order and time delay of the model are determined first, the rational parameters of the model are then determined by minimizing a quadratic loss function defined by the mean-squared errors between the sampled data and predicted data. That is to say, the resulting model is an optimal choice for dynamic model tracking. The outputs under the same PRBS and bode diagrams for models from various sampling interval are shown in Fig. 7. It can be seen that models with different time delay has similar outputs in the time domain and their phase frequency characteristics are almost identical in the low frequency. Despite the differences in the estimated time delay and fit ratios, the dynamic responses of the estimated models based on different sampling intervals are similar and they can all reflect the dynamic characteristics of the WPT system well.

2) Controller Performance: Subsequently, the internal model controller is designed based on the first-order model (26). The control period is the same as their sampling period. It can be seen from Figs. 8 and 9 that controller performance based on different sampling time are similar when the reference output voltage changes and λ is the same.

In addition to comparing the effect of the controller at different sampling intervals, the effect of λ is also considered in the experiment. When λ is set to 2e-3, the overshoot of the regulation

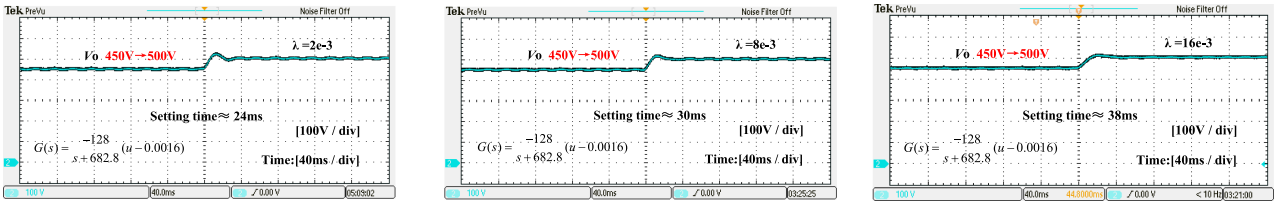

(a) (b) (c)

Fig. 11. V_o control experiment for the reference voltage rises for different λ, when $T_s = 0.8$ms, $\tau = 1.6$ms. (a) $\lambda = 2e-3$. (b) $\lambda = 8e-3$. (c) $\lambda = 16e-3$.

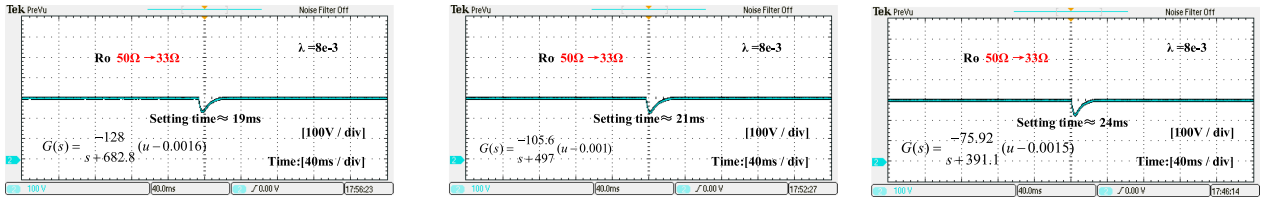

(a) (b) (c)

Fig. 12. V_o control experiment for R_o change. (a) $T_s = 0.8$ ms. (b) $T_s = 1.0$ ms. (c) $T_s = 1.5$ ms.

process is all greater than 0 and the voltage will fluctuate slightly around 450 V in Fig. 10. When λ is set to 8e-3. There is no overshoot and the setting time is satisfactory (about 20 ms). The output voltage is also very stable. When λ is set to 16e-3, the setting time becomes larger. It can be seen in Fig. 11 that the effect of λ is similar when the reference voltage rises.

The sharp change of the load resistance was implemented by removing one of the parallel resistance via opening the air breaker. For example, a load resistance change of 50 to 33Ω is realized in this article. The regulating process of the output voltage is depicted in Fig. 12. The setting time is about 19, 21, and 24 ms for various cases.

V. Conclusion

A new strategy was developed for modeling and control for WPT systems with time delay. This approach is user-friendly and convenient because it is based on experimental data, which is easy to obtain. Since the model parameters is decided by minimizing the error between the collected output and the simulated model output, the acquired model is suitable for dynamic model tracking and controller design.

Subsequently, a new procedure has been proposed that is a combination of the data-driven modeling method and IMC. According to simulation and experimental results, the length of the sampling time influences the accuracy of the time delay estimation, which is reflected in the fit ratio. However, the dynamic behavior of the model are determined by the combination of the model's time delay as well as the rational parameters. The resulting models with different time delays can all well reflect the dynamic behavior of the WPT system. In the control experiments, the various models all can achieve the desired control performance. The effect of λ is also explored. When λ is set to be $8e^{-3}$, the setting time of the regulating process is about 20 ms without overshoot.

References

[1] A. Kurs, "Wireless power transfer via strongly coupled magnetic resonances," *Science*, vol. 317, pp. 83–86, 2017.

[2] B. L. Cannon, J. F. Hoburg, D. D. Stancil, and S. C. Goldstein, "Magnetic resonant coupling as a potential means for wireless power transfer to multiple small receivers," *IEEE Trans. Power Electron.*, vol. 24, no. 7, pp. 1819–1825, Jul. 2009.

[3] G. A. Covic and J. T. Boys, "Inductive power transfer," *Proc. IEEE*, vol. 101, no. 6, pp. 1276–1289, 2013.

[4] S. Li and C. C. Mi, "Wireless power transfer for electric vehicle applications," *IEEE Trans. Emerg. Sel. Topics Power Electron.*, vol. 3, no. 1, pp. 4–17, Mar. 2015.

[5] L. Rubino, C. Capasso, and O. Veneri, "Review on plug-in electric vehicle charging architectures integrated with distributed energy sources for sustainable mobility," *Appl. Energy*, vol. 207, pp. 438–464, 2017.

[6] K. Agarwal, R. Jegadeesan, Y.-X. Guo, and N. V. Thakor, "Wireless power transfer strategies for implantable bioelectronics," *IEEE Rev. Biomed. Eng.*, vol. 10, pp. 136–161, 2017.

[7] C. C. Mi, G. Buja, S. Y. Choi, and C. T. Rim, "Modern advances in wireless power transfer systems for roadway powered electric vehicles," *IEEE Trans. Ind. Electron.*, vol. 63, no. 10, pp. 6533–6545, Oct. 2016.

[8] H. H. Lee, S. H. Kang, and C. W. Jung, "MR-WPT with reconfigurable resonator and ground for laptop application," *IEEE Microw. Wireless Compon. Lett.*, vol. 28, no. 3, pp. 269–271, Mar. 2018.

[9] A. P. Sample, D. T. Meyer, and J. R. Smith, "Analysis, experimental results, and range adaptation of magnetically coupled resonators for wireless power transfer," *IEEE Trans. Ind. Electron.*, vol. 58, no. 2, pp. 544–554, Feb. 2011.

[10] F. Chen, H. Garnier, Q. Deng, M. K. Kazimierczuk, and X. Zhuan, "Control-oriented modeling of wireless power transfer systems with phase-shift control," *IEEE Trans. Power Electron.*, vol. 35, no. 2, pp. 2119–2134, Feb. 2020.

[11] Y. Jiang, L. Wang, Y. Wang, J. Liu, X. Li, and G. Ning, "Analysis, design, and implementation of accurate ZVS angle control for EV battery charging in wireless high-power transfer," *IEEE Trans. Ind. Electron.*, vol. 66, no. 5, pp. 4075–4085, May 2019.

[12] H. Li, K. Wang, L. Huang, W. Chen, and X. Yang, "Dynamic modeling based on coupled modes for wireless power transfer systems," *IEEE Trans. Power Electron.*, vol. 30, no. 11, pp. 6245–6253, Nov. 2015.
[13] Y. Chen, W. Xiao, Z. Guan, B. Zhang, D. Qiu, and M. Wu, "Nonlinear modeling and harmonic analysis of magnetic resonant WPT system based on equivalent small parameter method," *IEEE Trans. Ind. Electron.*, vol. 66, no. 8, pp. 6604–6612, Aug. 2019.
[14] Z.-J. Liao, Y. Sun, Z.-H. Ye, C.-S. Tang, and P.-Y. Wang, "Resonant analysis of magnetic coupling wireless power transfer systems," *IEEE Trans. Power Electron.*, vol. 34, no. 6, pp. 5513–5523, Jun. 2019.
[15] P. C. Young, *Recursive Estimation and Time-Series Analysis: An Introduction for the Student and Practitioner*. Berlin, Germany: Springer-Verlag, 2011.
[16] L. Ljung, "Identification for control: Simple process models," in *Proc. 41st IEEE Conf. Decis. Control*, 2002, pp. 4652–4657 .
[17] T. Söderström and P. Stoica, *Instrumental Variable Methods for System Identification*. New York, NY, USA: Springer-Verlag, 1983.
[18] P. C. Young and A. J. Jakeman, "Refined instrumental variable methods of recursive time-series analysis—Part III: Extensions," *Int. J. Control*, vol. 31, no. 4, pp. 741–764, 1980.
[19] Z. Qiu, M. Santillo, M. Jankovic, and J. Sun, "Composite adaptive internal model control and its application to boost pressure control of a turbocharged gasoline engine," *IEEE Trans. Control Syst. Technol.*, vol. 23, no. 6, pp. 2306–2315, Nov. 2015.
[20] M. K. Kazimierczuk and D. Czarkowski, *Resonant Power Converters*. New York, NY, USA: Wiley, 2011.
[21] Q. Deng *et al.*, "Multi-inverter phase-shifted control for IPT with overlapped transmitters," *IEEE Trans. Power Electron.*, vol. 36, no. 8, pp. 8799–8811, Aug. 2021.
[22] H. Garnier and L. Wang, *Identification of Continuous-Time Models*. London, U.K.: Springer-Verlag, 2008.

Qijun Deng received the B.S and M.Sc. degrees in mechanical engineering and the Ph.D. degree in computer application technology from Wuhan University, Wuhan, China, in 1999, 2002, and 2005, respectively.

In June 2005, he joined the Department of Automation (which now is merged with the School of Electrical Engineering and Automation), Wuhan University, where he is currently a Professor. From 2013 to 2014, he was a Visiting Scholar with New York University Tandon School of Engineering. His research interests include wireless power transfer, distribution automation, and electrical power informatics.

Zhifan Li received the B.S. degree in automation in 2019 from Wuhan University, Wuhan, China, where he is currently working toward the M.Sc. degree with the School of Electrical Engineering and Automation.

His current research interests include the areas of wireless power transfer and system identification.

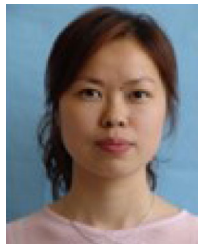

Jiangtao Liu received the B.S. and M.Sc. degrees in control theory and applications and the Ph.D. degree in electrical engineering from Wuhan University, Wuhan, China, in 1999, 2008, and 2013, respectively.

In June 2003, she joined the School of Physical, Mechanical and Electrical Engineering. From 2013 to 2014, she was a Visiting Scholar with the New York University Tandon School of Engineering. She is currently a Professor with the Hubei University of Education, Wuhan, China. Her research interests include wireless power transfer and noise reduction for power transformers.

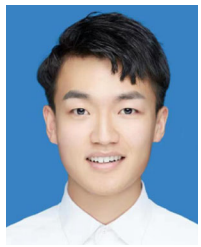

Shuaiqi Li received the B.S. degree in automation in 2019 from Wuhan University, Wuhan, China, where he is currently working toward the Ph.D. degree with the School of Electrical Engineering and Automation.

His research interests include the areas of wireless power transfer.

Peng Luo received the B.S. degree in automation in 2021 from Wuhan University, Wuhan, China, where he is currently working toward the M.Sc. degree with the School of Electrical Engineering and Automation.

His research interests include the areas of wireless power transfer.

Kaicong Cui received the B.S. degree in automation in 2021 from Wuhan University, Wuhan, China, where he is currently working toward the M.Sc. degree with the School of Electrical Engineering and Automation.

His research interests include the areas of wireless power transfer.